A photo-curable gel electrolyte ink for 3D-printable quasi-solid-state lithium-ion batteries

COMMUNICATION

A photo-curable gel electrolyte ink for 3D-printable quasi-solid-state lithium-ion batteries

Yoshiyuki Gambe, Hiroaki Kobayashi*, Kazuyuki Iwase, Sven Stauss, and Itaru Honma*

3D printing technologies have been adapted to enable the fabrication of lithium-ion batteries (LIBs), allowing flexible designs such as micro-scale 3D shapes. Here, we developed and studied 3D-printable gel electrolytes, at room temperature. The electrolyte gel solidified by UV irradiation maintains its structural integrity and high lithium-ion conductivity, enabling fully 3D-printed quasi-solid-state LIBs.

All-solid-state lithium-ion batteries (LIBs) have attracted great interest as potentially safe storage systems when compared to commercial batteries that use flammable organic liquid electrolytes.[1-7] Moreover, in recent years, 3D printing technologies have been adapted to enable the fabrication of LIBs,[8-10] thereby allowing the convenient production of flexible designs, such as micro-scale 3D shapes. In principle, such micro-batteries can be directly integrated onto a substrate that contains various electronic devices, using a simple printing system. Recently, 3D printable ink for LIB's cathode and anode have been made available.[8-13] Working on this, Lewis *et al*. realized that lithium-ion microbatteries made by using 3D printable electrode inks had properly tuned rheological and electrochemical characteristics.[8] Kohlmeyer *et al*. developed LiFePO$_4$ and LiCoO$_2$ (LCO) inks for the cathode and Li$_4$Ti$_5$O$_{12}$ (LTO) inks for the anode.[11] These inks consist of materials commonly used for electrode preparation: active materials, carbon nanofibers, poly(vinylidene fluoride) (PVDF), and *N*-methyl-2-pyrrolidone (NMP). Printable electrolyte inks are also important for printing complete batteries, and some research groups have reported on printable electrolytes, as summarized in Table S1.[14-18] Cheng *et al*. developed a 3D-printable hybrid solid-state electrolyte for LIBs using an elevated-temperature direct-ink writing technique.[15] The electrolyte ink consisted of lithium bis(trifluoromethanesulfonyl) imide (Li-TFSI) dissolved in *N*-propyl-*N*-methylpyrrolidinium

bis(trifluoromethanesulfonyl)imide (Pyr13-TFSI) as a lithium-conducting ionic liquid, titanium oxide (TiO$_2$) as an additive to tune the rheology, and poly(vinylidene fluoride-hexafluoropropylene) (PVDF-*co*-HFP). The electrolyte ink was extruded from a heated nozzle (at 120 °C) and subsequently cooled to room temperature to solidify. In addition to LIBs, reports suggest that printable electrolytes can be used for electrochemical devices such as electrochemical capacitors.[19, 20] In all such reports, printable electrolytes were mainly adapted for inkjet-, stencil-, or screen-printing, and there has been little research on applying gel electrolytes to 3D printing; this could potentially enable layered and more complex electrolyte structures. Furthermore, to the best of our knowledge, 3D-printable electrolyte extrusion at room temperature has not yet been considered.

In this study, we developed 3D-printable, UV-curable gel electrolyte inks to achieve fully 3D-printed quasi-solid-state LIBs. In principle, gel electrolyte inks can be printed directly onto various support structures, including soft substrates, without any heating process; this enables the simple and direct fabrication of electronic devices containing thermally unstable nanomaterials that can be used in biocompatible sensors.[21] The 3D-printable electrolyte inks were fabricated by adding UV-curable polymers to ion gels[22] consisting of a lithium-conducting ionic liquid and silica nanoparticles. Recently, we developed a direct printable proton conducting membrane (PCM) consisting of a UV-curable polymer, a proton-conducting ionic liquid, and silica nanoparticles.[23] This printable PCM enables the operation and testing of a quasi-solid-state electrochemical double-layer capacitor. In this study, 1 M Li-TFSI dissolved in 1-ethyl-3-methyl imidazolium bis(trifluoromethanesulfonyl)imide (EMI-TFSI) was selected as the lithium-conducting ionic liquid, since this mixture has been thoroughly investigated as an electrolyte for both LIBs[24] and quasi-solid-state batteries.[25] We optimized the concentration of silica nanoparticles to achieve good structural stability during material stacking. To then evaluate the possibility of applying the mixture to 3D printing, we deposited line and cylindrical structures using a custom-built 3D printer.

Using the optimized 3D-printable electrolyte inks, quasi-solid-state LIBs were assembled by applying a LCO slurry-coated cathode and a Li metal foil anode, as shown in Scheme 1. Furthermore, fully 3D-printed quasi-solid-state LIBs were assembled using 3D-printable LCO cathode and LTO anode electrode inks, as discussed in a previous report.[11] The properties of 3D printable electrolyte inks are discussed based on their rheological, ionic transport, and 3D structural properties. The charge and discharge performances of both the quasi-solid-state cells and fully 3D-printed cells were also investigated.
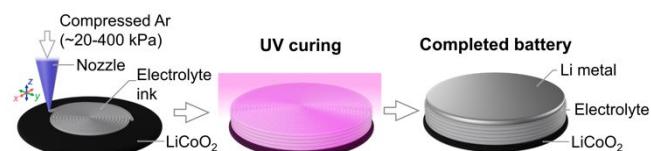
Scheme 1. Illustration of 3D printing of gel electrolyte inks, UV curing and geometry of the completed quasi-solid-state LIB.

Fig. 1a shows the appearance of gels composed of 1 M Li-TFSI/EMI-TFSI, silica nanoparticles, and UV-curable polymers; detailed synthesis and fabrication procedures are summarized in Fig. S1. Gelation was observed with the addition of 3–7 wt% silica nanoparticles, and quasi-solidification occurred with the addition of 10 wt% nanoparticles. To investigate the rheological properties of the fabricated gel electrolytes, viscosity measurements were performed on the gel electrolytes as a function of the silica concentration (see Fig. S2). For gel electrolytes with concentrations of 3–7 wt%, viscosity tended to decrease as the shear rate increased; a similar tendency was observed in the ion gels without UV-curable polymer.[22] Rheology measurements revealed that the fabricated gel electrolytes exhibit non-Newtonian fluid behavior, which is similar to previously reported 3D-printable cathode and anode electrode inks.[8, 11, 13] Fig. 1b shows these viscosities at a shear rate of 10 s^{-1}, and the ionic conductivities of the gel electrolytes before and after UV irradiation as a function of SiO$_2$ concentration; viscosity tended to increase as the concentration of SiO$_2$ increased. Ueno *et al*. revealed that the strong electrostatic interaction at the ionic liquid-silica interface increases the viscosity of the ionic liquid by 1–3 orders of magnitude.[26] From this it can be considered that the viscosity of the fabricated gel electrolyte rises because the nanoparticle interface increases with an increase in the amount of SiO$_2$ nanoparticles. Regarding the ionic conductivity of the gel electrolytes with 3–7 wt% of SiO$_2$ nanoparticles, it was found that the ionic conductivity was almost constant, regardless of the SiO$_2$ concentration. Additionally, there was no significant decrease in the ionic conductivity of the solidified sample following UV irradiation, and this behavior remained similar over the entire temperature range (see Fig. S3). The ionic conductivity of the solidified electrolyte, prepared at a silica concentration of 7 wt%, was as high as 2.9 × 10^{-3} S cm^{-1} at 25 °C. Fig. 1c shows the self-diffusion coefficients of H-, F-, and Li-containing species of gel electrolyte inks before and after UV

irradiation; ^1H and ^{19}F correspond to the diffusion of EMI cations and TFSI anions, respectively. It was found that the values of all diffusing species were similar before and after UV irradiation, regardless of the SiO$_2$ concentration, this showing the same tendency as the ionic conductivity. As shown in Fig. S4, the relative diffusivity (D_x/D_0) of the lithium-ion and the lithium-ion transport number (t_{Li+}) before and after UV irradiation also indicated no change. Based on all this, a gel electrolyte ink with an optimal viscosity for 3D printing can be developed by adding a small amount of oxide nanoparticles with a high specific surface area, and high lithium-ion transport characteristics can be maintained even after UV curing.
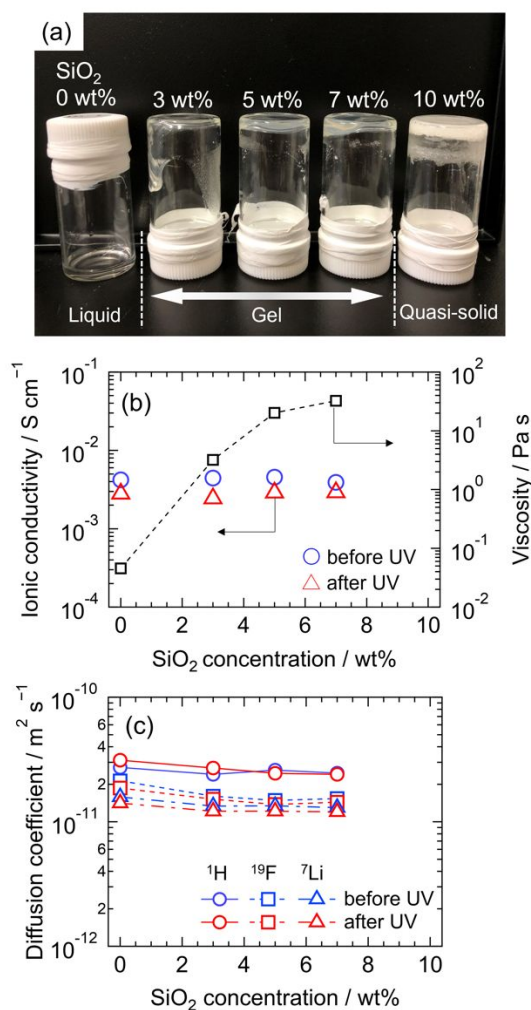

Fig. 1. (a) Photographs of electrolyte inks consisting of ionic liquid, UV-curable polymer, and SiO$_2$ nanoparticles. (b) SiO$_2$ concentration dependencies of ionic conductivity and viscosity. (c) SiO$_2$ concentration dependencies of the self-diffusion coefficients of ^1H, ^{19}F and ^7Li species in the gel electrolytes inks before and after UV-irradiation.

We fabricated line- and cylindrically-shaped geometries to evaluate whether the 3D-printed electrolytes maintained their shape and ionic conductivity even after stacking. For this, a custom-made 3D printer placed inside an Ar-filled glove box was used. A movie of a typical 3D printing process of the gel electrolyte can be found entitled "Supporting Movie 1". Fig. 2a shows a scanning electron microscope (SEM) image of the line-

COMMUNICATION

shaped gel electrolyte with 7 wt% SiO_2 nanoparticles after UV curing, which exhibited the best structural stability. Accoding to the photodifferential scanning calorimetry (Photo-DSC) quantitative analysis,[27] 64(1)% of monomers were polymerized following UV light irradiation. This value was sufficient to ensure the solidification of the printed lines, and higher than that of our previous work on PCMs, where 8% of UV-curable resin was polymerized.[23] The higher polymerization ratio is probably due to lower SiO_2 content (7wt% in this work, 27.5wt% in PCM) which possibly scatters UV-light. The gel electrolytes maintained their shape without collapsing, even after extrusion from a 3D printer nozzle with a nominal opening of 200 µm, and this study succeeded in depositing smooth and continuous lines at equal intervals. From the 3D laser microscope measurements displayed in Fig. 2b, it was found that lines with a width of approximately 240 µm and a height of approximately 175 µm could be extruded. Fig. 2c shows the variation in the line width and height of vertically stacked lines printed successively on top of each other from layers 1 to 5. As the number of layers increased, the line width remained almost constant, and the line height tended to show a linear increase. The inset in Fig. 2c shows the SEM observation of a 3D-printed and solidified electrolyte structure, consisting of 5-layers viewed from the top and the side. It was found that the line width did not increase even for 5 layers, and the line width remained constant at approximately 280 µm. In addition, from cross-sectional SEM observations, it was confirmed that the lines could be closely stacked in 5 layers with a height of approximately 960 µm, which was approximately five times the height of a 1-layer line. Based on this, 3D-printable gel electrolyte inks can be developed that can maintain their structure even when laminated and extruded. Fig. 2d shows the ionic conductivities of the samples solidified by UV irradiation after 3D printing of 1 to 5 layers of cylindrical electrolyte membranes with a diameter of 5 mm. Compared to a standard electrolyte (indicated as a black dotted line), the printed electrolytes with 1 to 5 printed layers show almost no decrease in the ionic conductivity, and were found to show a high ionic conductivity of about 2×10^{-3} S cm^{-1}. Since the electrolyte membrane was made from multiple extruded lines with a width of approximately 240 µm and a height of approximately 175 µm, the number of interfaces is larger than that of molded membranes. However, almost no contact resistance was observed, and the 3D-printable electrolytes showed good adhesion.
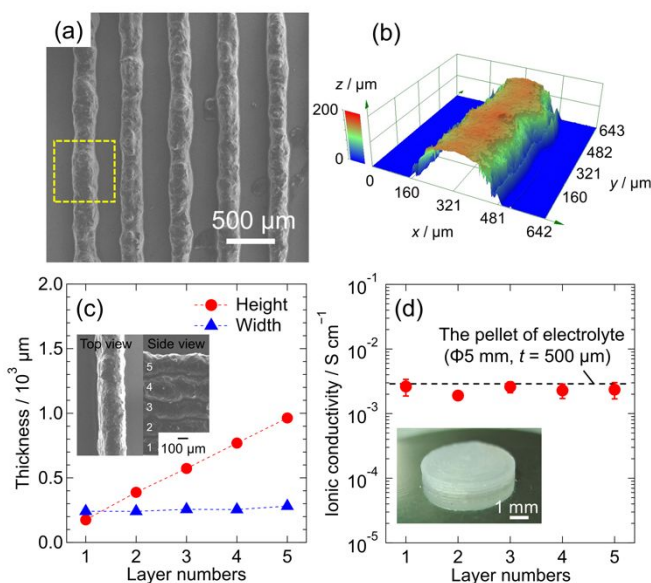

Fig. 2. (a) SEM image and (b) 3D laser microscope image of a printed electrolyte gel. The yellow dashed square in (a) represents the area of the 3D image. (c) Heights and widths of 3D-printed electrolyte inks as function of the number of printed layers. Inset shows SEM images of top and side views of 3D-printed and solidified 5-layer electrolyte structure. (d) Ionic conductivities of the 3D-printed electrolyte inks as a function of the number of layers. The dashed black line indicates the ionic conductivity of a dense gel electrolyte pellet with a diameter of 5 mm and 500 µm thickness. Photograph of the 3D-printed gel electrolyte consisting of 4 stacked circles is inserted.

For tests on the quasi-solid-state LIB half-cells, an LCO slurry-coated electrode was used as the cathode and a Li metal foil was used as the anode. The gel electrolyte was printed on the LCO cathode sheet using the 3D printing sequence shown in Fig. S5a and Supporting Movie 2, before placing the Li metal anode on top. Fig. 3a shows the specific charge/discharge curves of a quasi-solid-state LCO/Li half-cell, with a printed electrolyte at a current rate of 0.1 C. The redox reaction plateaus at approximately 3.9 V, which are typical for LCO cathodes, are observed with low polarization (Fig. S6), indicating almost no interface resistance of the printed electrolyte. The initial discharge capacity was approximately 100 mAh g^{-1}, with a Coulombic efficiency of 73%. The Coulombic efficiency increased to 90% after the initial cycles, while maintaining the discharge capacity. This indicates that electrolyte decomposition occurs slightly in the initial charge cycles without degrading the cell performance. Fig. 3b shows the discharge capacities and Coulombic efficiencies of the quasi-solid-state cell with the printed electrolyte as a function of the number of charge/discharge cycles at 35 °C. At a C-rate of 0.1 C, the cell exhibited good cycling capability. As the C-rate increased, the capacity degradation became more marked, and the polarization of the redox plateau at the higher C-rate rapidly increased during cycles (Fig. S7). Since the printed electrolyte has a sufficient ionic conductivity (Fig. 2d), the lower cyclability at the higher C-rate is probably due to solid-electrolyte interface (SEI) film growth during cycles, formed by side reactions between the lithium metal and the printed electrolyte, that occurred preferentially because of the increase in current density, as detailed in our previous study.[25] According to this,

our quasi-solid-state cell allowed successful battery operation at lower C-rates. As shown in Fig. S8, the quasi-solid-state LIB realized with 3D-printed, 5-layer electrolytes also exhibited a high discharge capacity equivalent to that consisting of a 1-layer electrolyte, with little change in the polarization. These battery performances are similar to those of previously reported quasi-solid-state LIBs,[25] where the battery cell test conditions were almost the same, except that they contained a higher concentration of SiO_2 and polytetrafluoroethylene (PTFE) binder in the electrolyte instead of UV-curable polymers. Slight differences in the reversible capacity and rate capability are derived from the utilization ratio of the active materials, affected by the specific contact surface area of the electrolyte.
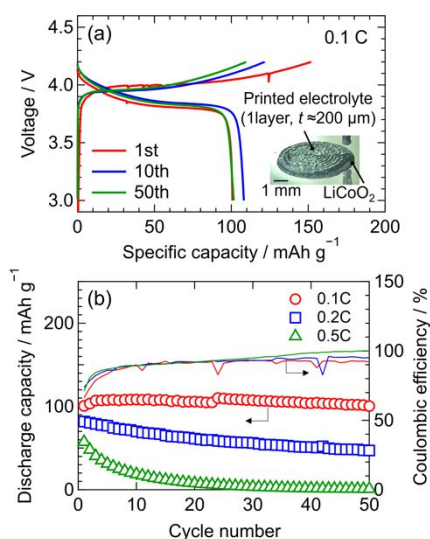

Fig. 3. (a) Charge/discharge profiles and (b) discharge capacities and coulombic efficiencies of the quasi-solid-state LCO/Li half-cell with printed electrolyte.

A fully 3D-printed quasi-solid-state LIB full-cell was fabricated, as shown in Fig. 4a. The viscosities of the LCO and LTO electrode inks were approximately 100 and 300 Pa s at a shear rate of 10 s^{−1}, respectively, and electrodes were similarly printed with line widths of 380 and 490 μm (see Fig. S9). The impedance spectrum during charging (see Fig. 4b) shows four resistance components with a Warburg impedance (W). These resistance components are attributable to the solution resistance (R_S, an offset of the Z'-axis), charge transfer resistance at the LTO anode ($R_{CT,LTO}$, a semicircle in the high-frequency region), SEI film (R_{SEI}, a small semicircle in the medium-frequency region), and charge-transfer resistance at the LCO cathode ($R_{CT,LCO}$, a semicircle in the low-frequency region).[28] The SEI likely derives from the UV-curable polymers contained in the inks, although this is unconfirmed. Fig. 4c shows the 1st, 10th, and 100th charge/discharge profiles of a fully 3D-printed LIB at a C-rate of 0.05 C. The terminal voltage of the LCO/LTO full cell was approximately 2.3 V; this charge/discharge profile matches the common result as previously reported[29] and shows less polarization effects (see Fig. S10). By demonstrating the battery operation of the fully 3D-printed LIB, the practicality of the printed electrolyte highlighted in this study was demonstrated. However, the 1st

discharge capacity was 52 mAh g^{−1}, with a cathode utilization ratio as low as 35 %, and the rate capability test showed that the charge/discharge operation at more than 0.1 C hardly proceeded (Fig. 4d). Because this evaluation of the LCO/LTO full cell was performed by adjusting the cathode and anode capacities to be almost the same, it is expected that the utilization ratio of the LCO cathode will be improved by optimizing the balance between the cathode and anode capacities. The utilization ratio can also be improved by electrode ink optimization, for example, by using carbon nanofibers instead of acetylene black.[11]
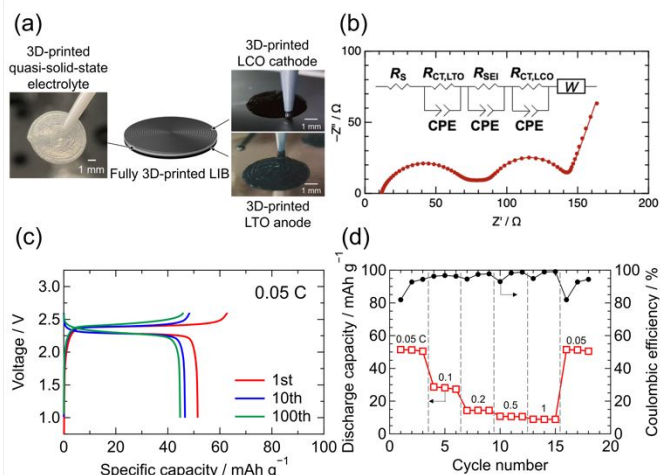

Fig. 4. (a) Photographs and illustration of the fully 3D-printed LCO/LTO full-cell using a printed electrolyte. Panels on the left and right display optical images of the 3D-printed-quasi-solid-state electrolyte, as well as the LCO and LTO electrodes. (b) Nyquist plot with fitting curve of a fully 3D-printed quasi-solid-state LCO/LTO full cell at a voltage of 2.34 V during charging at a C-rate of 0.05 C. The inset shows the equivalent circuit. (c) Charge/discharge profiles. (d) Result of the rate capability test.

We have succeeded in developing a 3D-printable gel-like electrolyte that enables extrusion printing at room temperature with good structural integrity even after stacking several layers, as well as the operation of fully 3D-printed quasi-solid-state LIBs. The approach presented here is expected to enable the simple fabrication of thermally unstable electronic devices, such as flexible devices and biocompatible micro-sensors.

CRediT author contributions

Y.G.: Conceptualization, Data curation, Formal Analysis, Funding acquisition, Investigation, Methodology, Writing − original draft; H.K.: Funding acquisition, Methodology, Project administration, Writing − review & editing; K.I.: Formal Analysis, Writing − review & editing; S.S.: Software, Writing − review & editing; I.H.: Funding acquisition, Supervision, Writing − review & editing.

Conflicts of interest

There are no conflicts to declare.

Acknowledgements

Notes and references

1   M. Armand and J. M. Tarascon, *Nature*, 2008, **451**, 652-657.
2   J. B. Goodenough and K.-S. Park, *J. Am. Chem. Soc.*, 2013, **135**, 1167-1176.
3   C. Sun, J. Liu, Y. Gong, D. P. Wilkinson and J. Zhang, *Nano Energy*, 2017, **33**, 363-386.
4   W. Zhang, J. Nie, F. Li, Z. L. Wang and C. Sun, *Nano Energy*, 2018, **45**, 413-419.
5   S. Li, D. Zhang, X. Meng, Q.-A. Huang, C. Sun and Z. L. Wang, *Energy Stor. Mater.*, 2018, **12**, 17-22.
6   G. Qiu and C. Sun, *New J. Chem.*, 2020, **44**, 1817-1824.
7   L. Liu and C. Sun, *ChemElectroChem*, 2020, **7**, 707-715.
8   K. Sun, T.-S. Wei, B. Y. Ahn, J. Y. Seo, S. J. Dillon and J. A. Lewis, *Adv. Mater.*, 2013, **25**, 4539-4543.
9   T.-S. Wei, B. Y. Ahn, J. Grotto and J. A. Lewis, *Adv. Mater.*, 2018, **30**, 1703027.
10 S. Praveen, P. Santhoshkumar, Y. C. Joe, C. Senthil and C. W. Lee, *Appl. Mater. Today*, 2020, **20**, 100688.
11 R. R. Kohlmeyer, A. J. Blake, J. O. Hardin, E. A. Carmona, J. Carpena-Núñez, B. Maruyama, J. Daniel Berrigan, H. Huang and M. F. Durstock, *J. Mater. Chem. A*, 2016, **4**, 16856-16864.
12 J. Hu, Y. Jiang, S. Cui, Y. Duan, T. Liu, H. Guo, L. Lin, Y. Lin, J. Zheng, K. Amine and F. Pan, *Adv. Energy Mater.*, 2016, **6**, 1600856.
13 D. Cao, Y. Xing, K. Tantratian, X. Wang, Y. Ma, A. Mukhopadhyay, Z. Cheng, Q. Zhang, Y. Jiao, L. Chen and H. Zhu, *Adv. Mater.*, 2019, **31**, 1807313.
14 D. W. McOwen, S. Xu, Y. Gong, Y. Wen, G. L. Godbey, J. E. Gritton, T. R. Hamann, J. Dai, G. T. Hitz, L. Hu and E. D. Wachsman, *Adv. Mater.*, 2018, **30**, 1707132.
15 M. Cheng, Y. Jiang, W. Yao, Y. Yuan, R. Deivanayagam, T. Foroozan, Z. Huang, B. Song, R. Rojaee, T. Shokuhfar, Y. Pan, J. Lu and R. Shahbazian-Yassar, *Adv. Mater.*, 2018, **30**, 1800615.
16 S.-H. Kim, K.-H. Choi, S.-J. Cho, J. Yoo, S.-S. Lee and S.-Y. Lee, *Energy Env. Sci.*, 2018, **11**, 321-330.
17 S.-H. Kim, J.-H. Kim, S.-J. Cho and S.-Y. Lee, *Adv. Energy Mater.*, 2019, **9**, 1901841.
18 P. E. Delannoy, B. Riou, B. Lestriez, D. Guyomard, T. Brousse and J. Le Bideau, *J. Power Sources*, 2015, **274**, 1085-1090.
19 S.-S. Lee, K.-H. Choi, S.-H. Kim and S.-Y. Lee, *Adv. Funct. Mater.*, 2018, **28**, 1705571.
20 C. Chae, J. H. Han, S. S. Lee, Y. Choi, T.-H. Kim and S. Jeong, *Adv. Funct. Mater.*, 2020, **30**, 2000715.
21 S. Stauss and I. Honma, *Bull. Chem. Soc. Jpn.*, 2018, **91**, 492-505.
22 K. Ueno, K. Hata, T. Katakabe, M. Kondoh and M. Watanabe, *J. Phys. Chem. B*, 2008, **112**, 9013-9019.
23 K. Iwase, S. Stauss, Y. Gambe, R. Miyazaki and I. Honma, *ACS Appl. Energy Mater.*, 2021, **4**, 3651-3659.
24 B. Garcia, S. Lavallée, G. Perron, C. Michot and M. Armand, *Electrochim. Acta*, 2004, **49**, 4583-4588.
25 A. Unemoto, H. Ogawa, S. Ito and I. Honma, *J. Electrochem. Soc.*, 2013, **160**, A138-A147.
26 K. Ueno, M. Kasuya, M. Watanabe, M. Mizukami and K. Kurihara, *Phys. Chem. Chem. Phys.*, 2010, **12**, 4066-4071.
27 T. Uehara, S. Sato, S. Ito, H. Yano, T. Nakamura and M. Nakagawa, *Bull. Chem. Soc. Jpn.*, 2018, **91**, 178-186.
28 N. Schweikert, R. Heinzmann, A. Eichhöfer, H. Hahn and S. Indris, *Solid State Ionics*, 2012, **226**, 15-23.
29 A. M. Gaikwad, B. V. Khau, G. Davies, B. Hertzberg, D. A. Steingart and A. C. Arias, *Adv. Energy Mater.*, 2015, **5**, 1401389.